RESEARCH ARTICLE

National Science Review
11: nwae031, 2024
https://doi.org/10.1093/nsr/nwae031
Advance access publication 22 January 2024

CHEMISTRY

On-surface synthesis and characterization of polyynic carbon chains

Wenze Gao, Wei Zheng, Luye Sun, Faming Kang, Zheng Zhou and Wei Xu*

ABSTRACT

Carbyne, an elusive *sp*-hybridized linear carbon allotrope, has fascinated chemists and physicists for decades. Due to its high chemical reactivity and extreme instability, carbyne was much less explored in contrast to the sp^2-hybridized carbon allotropes such as graphene. Herein, we report the on-surface synthesis of polyynic carbon chains by demetallization of organometallic polyynes on the Au(111) surface; the longest one observed consists of ∼60 alkyne units (120 carbon atoms). The polyynic structure of carbon chains with alternating triple and single bonds was unambiguously revealed by bond-resolved atomic force microscopy. Moreover, an atomically precise polyyne, C_{14}, was successfully produced via tip-induced dehalogenation and ring-opening of the decachloroanthracene molecule ($C_{14}Cl_{10}$) on a bilayer NaCl/Au(111) surface at 4.7 K, and a band gap of 5.8 eV was measured by scanning tunnelling spectroscopy, in a good agreement with the theoretical HOMO–LUMO gap (5.48 eV).

Keywords: polyyne, scanning probe microscopy, carbon allotrope, on-surface synthesis, organometallic polyyne

INTRODUCTION

The creation of new carbon forms with different topologies has emerged as an exciting topic in both fundamental chemistry and materials science. Since the first discovery of fullerenes [1], carbon nanotubes (CNTs) [2,3], and graphene [4], the family of sp^2 carbon allotropes have been broadly explored and investigated which exhibit unusual chemical and physical properties [5]. Some recent studies have enriched this family to seek new polymeric carbon forms, such as fullerene networks [6,7]. In contrast, carbyne, an *sp*-hybridized carbon allotrope with an infinite one-dimensional (1D) carbon chain attracted more interest back in the 1960s, but its structure remained controversial over the decades [8,9]. Unlike conventional 1D carbon allotrope CNTs, carbyne is a real ultimate 1D structure, which has a cross-sectional dimension reduced to only one carbon atom. Carbyne owns the potential to be the mechanically strongest known material due to its unique structure [10]. However, the great challenge of synthesizing accessible carbyne, caused by its high chemical reactivity and extreme instability, impeded the experimental confirmation and further exploration of its applications.

In principle, carbyne can be either polyynic with an alternation of single and triple bonds, or cumulenic with a connection of consecutive double bonds (Fig. 1a), while the former has been proven to be energetically more favorable [11]. Thus, the experimental attempts in this field have focused heavily on the synthesis of polyynes by different methods to model carbyne. In order to stabilize long carbon chains, adding endgroups is a common organic synthetic strategy for the preparation of polyyne with different lengths [12–17], and the longest polyyne reported so far consists of 24 contiguous alkyne units (48 carbons) [17]. However, longer polyynes commonly require heavier endgroups for stabilization, limiting the production of long polyynic carbon chains. Instead, single- and double-walled CNTs, known as confining nanoreactors and protectors to produce and stabilize highly active structures, have been used to prepare long carbon chains comprising more than 6000 carbon atoms [18].

On-surface synthesis is emerging as a promising approach for atomically precise fabrication of highly

Interdisciplinary Materials Research Center, School of Materials Science and Engineering, Tongji University, Shanghai 201804, China

*Corresponding author. E-mail: xuwei@tongji.edu.cn

Received 18 August 2023; **Revised** 16 December 2023; **Accepted** 18 December 2023

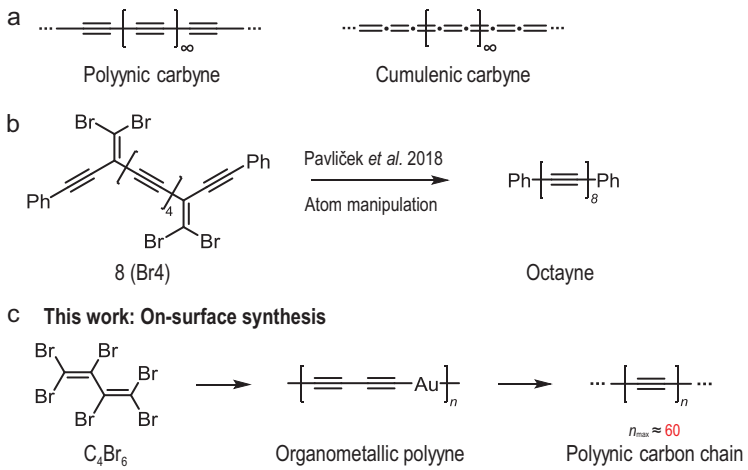

Figure 1. Synthetic strategies toward the polyynic carbon chain (PCC). (a) Two possible structures of carbyne. (b) Previous work towards the synthesis of polyyne compounds (with 8 alkyne units) by atomic manipulation on NaCl. (c) In this work, an on-surface synthesis strategy is applied where the C_4Br_6 precursor is employed to form PCC with the longest one observed consisting of ∼60 alkyne units.

reactive 1D nanostructures with *sp*-hybridization that could be hardly synthesized via conventional solution synthetic chemistry [19–22]. Developments in scanning tunneling microscopy (STM) and atomic force microscopy (AFM) have enabled the designing and *in-situ* characterization of low-dimensional carbon nanostructures with unprecedented resolution on the atomic scale and chemical-bond level [23–25]. Benefiting from the development of scanning probe microscopies above, a series of polyynes comprising 3, 4, 6, and 8 alkyne units have been successfully generated via skeletal rearrangement induced by atomic manipulation on NaCl at 5 K (Fig. 1b), and the polyynic structure was well-revealed by AFM [26]. However, its length is still limited by endgroups. Herein, we show how an on-surface synthesis approach can be developed to synthesize polyynic carbon chains (PCCs) without endgroups, and the longest one consists of ∼60 alkyne units. As shown in Fig. 1c, 1,1,2,3,4,4-hexabromobutadiene (C_4Br_6) molecules were first polymerized through debrominative coupling on the Au(111) surface followed by the formation of organometallic polyynes [20], and in the second step, these organometallic polyynes underwent demetallization by further annealing to form PCCs. A low-temperature STM/AFM was used to reveal the polyynic structure of carbon chains with bond-resolved resolution. Moreover, a specific C_{14} polyyne was also successfully produced via tip-induced dehalogenation and ring-opening of the decachloroanthracene molecule ($C_{14}Cl_{10}$) on a bilayer NaCl/Au(111) surface at 4.7 K. The electronic properties were further studied through a combination of scanning tunnelling spectroscopy (STS) and density functional theory (DFT) calculations, and a band gap of the C_{14} polyyne was measured to be 5.8 eV, in good agreement with the theoretical HOMO–LUMO gap (5.48 eV). Our results provide a feasible route for the synthesis of long and stable polyynic carbon chains by demetallization of organometallic polyynes on Au(111), and the on-surface generation of a carbon chain with a specific length on NaCl/Au(111) would be potentially useful for investigating the intrinsic properties of linear carbons.

RESULTS AND DISCUSSION

Synthesis and structural characterization

The C_4Br_6 was synthesized in solution through a two-step sequence (see Methods and Fig. S1 for synthetic details and NMR spectra) and then deposited onto a clean Au(111) surface held at 300 K in an ultrahigh vacuum, resulting in the formation of diacetylenic organometallic polyynes (−C≡C−C≡C−Au−) (Fig. 2, column 1) through debrominative organometallic coupling, which is similar to our previously reported work [20]. The bright protrusions in the STM image (Fig. 2a) resulted from the electronic density of states of Au atoms, as illustrated by the overlaid chemical structure in Fig. 2j. From the AFM images in Fig. 2g and m, the diyne moieties are clearly resolved as two discrete characteristic protrusions indicated by white arrows [25]. The distance between two C–C triple bonds is measured to be 2.62 Å (Fig. S2d).

The organometallic polyynes started to partially demetallize [27] as the sample was annealed to 380 K for 60 min, resulting in the formation of short PCCs within the organometallic polyynes (Fig. 2, column 2), in which the short PCC and the organometallic polyyne are outlined by white and blue contours in Fig. 2k, n, respectively. The bond-resolved AFM contrast provided conclusive evidence for a polyynic structure of PCCs with defined positions of triple bonds as indicated by white arrows in Fig. 2n with reference to the chemical structure overlaid in Fig. 2k [26]. The periodicity of PCCs is measured to be 2.56 Å (Fig. S2e) which corresponds well with the theoretical value (Fig. S3) and could be clearly distinguished from that of the acetylenic organometallic polyynes (5.20 Å) (Fig. S2c, f). Notably, within intermediate structures (Fig. 2, column 2), organometallic polyyne parts are not distinguishable in the AFM images at the imaging height of PCCs (Fig. 2n). This should

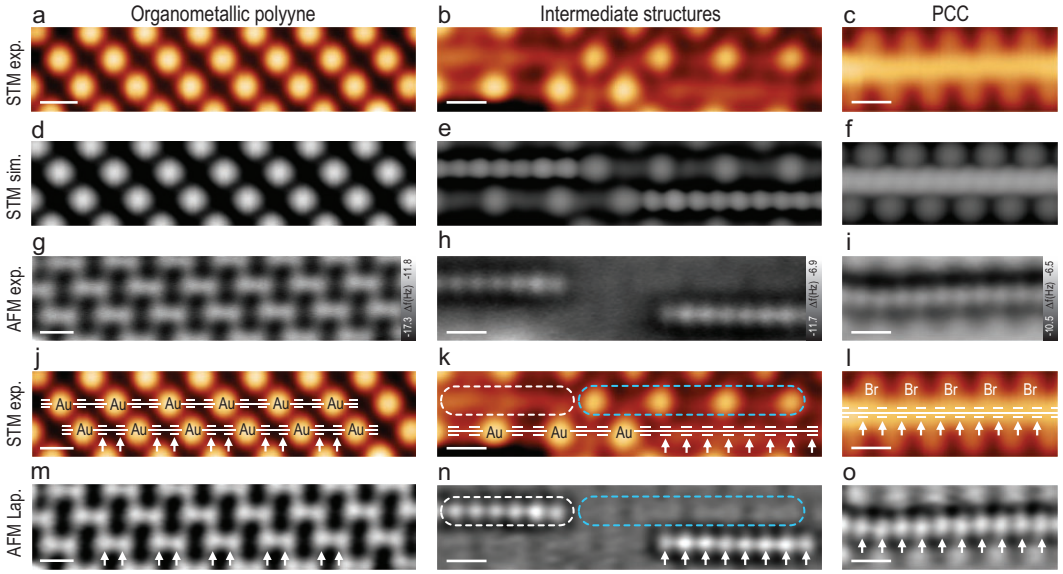

Figure 2. Formation of polyynic carbon chain by demetallization of organometallic polyyne. STM images (a–c, j–l), simulated STM images (d–f), AFM images (g–i), and Laplace-filtered AFM images (m–o) of organometallic polyynes, intermediate structures, and polyynic carbon chain, respectively. The STM images in (j–l) are overlaid with the chemical structures as guides. In the intermediate structure (k, n), the partially demetallized and the remaining organometallic polyyne are outlined by white and blue contours, respectively. The alkyne units are indicated by white arrows in (j–o). All STM images are taken at $V = 0.40$ V, $I_t = 100$ pA; all AFM images are recorded with a Br-functionalized tip at different tip offsets Δz (g: $\Delta z = -370$ pm, h: $\Delta z = -130$ pm, i: $\Delta z = -260$ pm) with respect to an STM set point ($V = 0.40$ V, $I_t = 100$ pA). Scale bars: 0.5 nm.

be attributed to the lower adsorption height of the organometallic polyyne due to stronger interaction with the substrate as compared to the PCC (Fig. S3). The PCCs became longer during further continuous annealing at 380 K for 120 min (Fig. 2, column 3). The AFM images (Fig. 2i, o) revealed a polyynic structure of PCC with a length of 12 alkyne units as illustrated by the chemical structure in Fig. 2l. The assignment of all products was further supported by STM simulations (Fig. 2d–f).

Longer PCCs with a length of at least 23 alkyne units (46 carbon atoms) were also observed (Fig. 3a), in which the defined positions of 23 triple bonds are nicely revealed by AFM imaging (Fig. 3b, c). The organometallic polyynes on both sides of PCC are not distinguishable in AFM images at the typical imaging height of PCC, which is in agreement with the situation in Fig. 2n. Significantly, the longest PCC we observed consists of ∼60 alkyne units (120 carbon atoms) based on its length (∼15 nm), as shown in Fig. 3d, e. It can be seen from the Laplace-filtered AFM image (Fig. 3e) that the structure of this PCC is still intact without defects, and the polyynic nature (characteristic protrusions originated from C–C triple bonds) remains visible. STM images of other representative PCCs with lengths of ∼7, 10 and 12 nm are shown in Fig. S4.

Electronic properties of PCCs

The electronic properties of PCCs were measured by STS. Due to the electronic coupling between the PCC and the metal surface, the detection of the electronic states was obscured and only the unoccupied state was detected at 1.17 V (Fig. S6). dI/dV maps acquired at this peak demonstrate that the corresponding state is highly localized at the PCC, without any characteristic feature (Fig. S6). More acutely, excessive Br adatoms resulting from the debromination of C_4Br_6 precursors affected the detection of the pure Au(111) surface states. As a result, a confined electronic state was detected at the centre of the pore surrounded by Br adatoms (Fig. S7) [28]. To obtain the intrinsic electronic properties of PCC, a partially decoupled one by intercalating Br atoms (indicated by the blue contour in Fig. 4a) was further characterized. The partially decoupled PCC segment exhibited a higher apparent height in the STM image (marked by the white contour in Fig. 4b) than the segment directly adsorbed on the metal substrate (marked by the black contour), as illustrated by the schematic model in Fig. 4d. This was further verified by the AFM image as the PCC segment on Au(111) was not imaged at the imaging height of the decoupled PCC segment (Fig. 4c). The close-up Laplace-filtered AFM image revealed that the de-

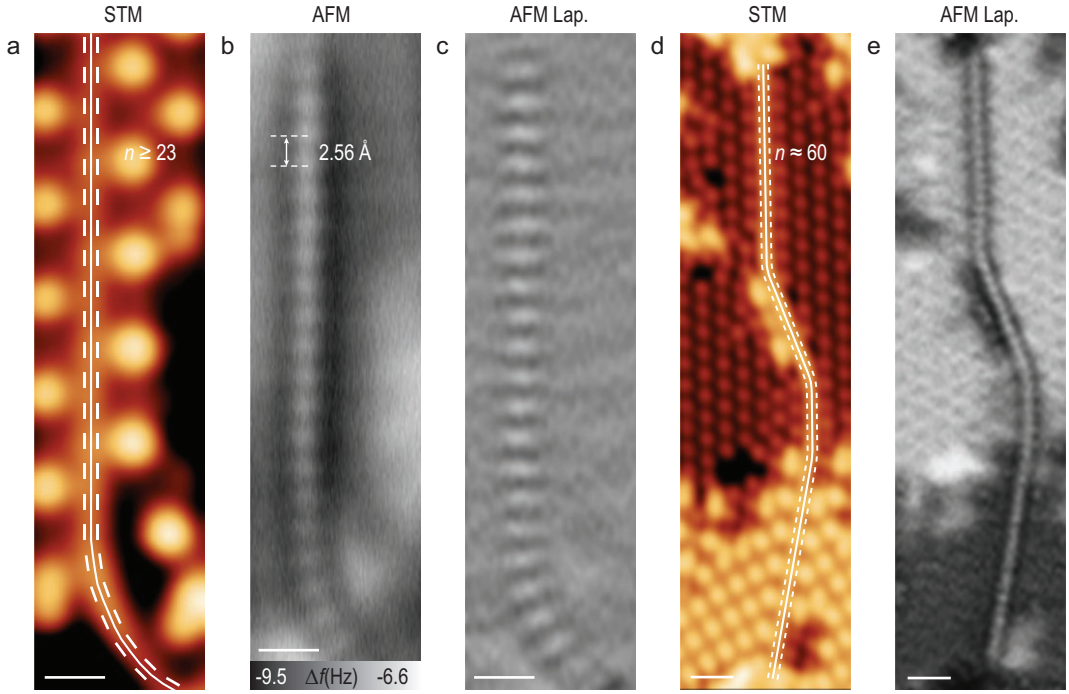

Figure 3. Real-space imaging of long polyynic carbon chains. (a–e) STM images (a, d), AFM images (b), and Laplace-filtered AFM images (c, e) of polyynic carbon chains with at least 23 (a–c) and ∼60 (d, e) alkyne units, respectively. The STM images in (a) and (d) are overlaid with the chemical structure as guides. The STM images are all taken at: $V = 0.40$ V, $I_t = 100$ pA. The AFM images are recorded with a Br-functionalized tip at different tip offsets Δz (b: $\Delta z = -75$ pm, e: $\Delta z = -80$ pm) with respect to an STM set point ($V = 0.40$ V, $I_t = 100$ pA). Scale bars: 0.5 nm (a–c); 1 nm (d–e).

coupled PCC segment consists of 10 alkyne units (Fig. S8).

A dI/dV spectrum taken at the decoupled PCC segment is shown in Fig. 4e. In contrast to the results on Au(111), this spectrum exhibits two resonance peaks at −2.8 V and 0.87 V, respectively, which can be assigned to the occupied and unoccupied states, resulting in a band gap of approximately 3.67 eV. The characteristic nodes shown in the middle of every triple bond in the PCC segment in the constant height dI/dV mapping acquired at 0.87 V are in agreement with DFT-calculated LUMO (Fig. S9).

C_{14} polyyne formation via atomic manipulation

To achieve a fully decoupled PCC and measure its intrinsic electronic property, another molecular precursor, decachloroanthracene ($C_{14}Cl_{10}$), was synthesized with the aim of generating a specific C_{14} carbon chain via tip-induced dehalogenation and ring-opening (Fig. 5a). $C_{14}Cl_{10}$ molecules were deposited onto a bilayer NaCl surface on Au(111) held at 6 K. To generate C_{14} polyyne, the tip was initially positioned on a single $C_{14}Cl_{10}$ molecule and retracted by about 4 Å from the STM set point ($I = 3$ pA, $V = 0.3$ V). Voltage pulses (4.0–4.5 V) were applied for a short duation (500 ms) at a constant tip height on the $C_{14}Cl_{10}$ molecule to induce full dehalogenation and accompanied ring opening. As a result, the polyynic C_{14} chain without endgroups was successfully generated as shown in the AFM images (Fig. 5b–d). According to the Laplace-filtered AFM image (Fig. 5c), seven characteristic protrusions can be clearly identified, attributed to seven C–C triple bonds as illustrated by the overlaid chemical structure in Fig. 5d, which could be unambiguously assigned to an individual C_{14} polyyne.

More importantly, because of decoupling by the insulating bilayer NaCl film, the intrinsic electronic property of C_{14} polyyne can be accurately characterized by STS with a CO-functionalized tip. Differential conductance spectrum (dI/dV) acquired on the C_{14} polyyne exhibits two pronounced peaks at –3.4 V and 2.4 V (Fig. 5e), corresponding to the positive and negative ion resonances (PIR and NIR), respectively, exhibiting a band gap of 5.8 eV, which is in a good agreement with the calculated HOMO–LUMO gap of the C_{14} polyyne (5.48 eV) at the ωB97XD/def2-TZVP level. Notably, the electronic properties of C_{14} polyyne can be significantly affected by the endgroups. Based on theoretical calculations, it is evident that the hydrogen-capped C_{14} polyyne possesses a larger HOMO–LUMO gap

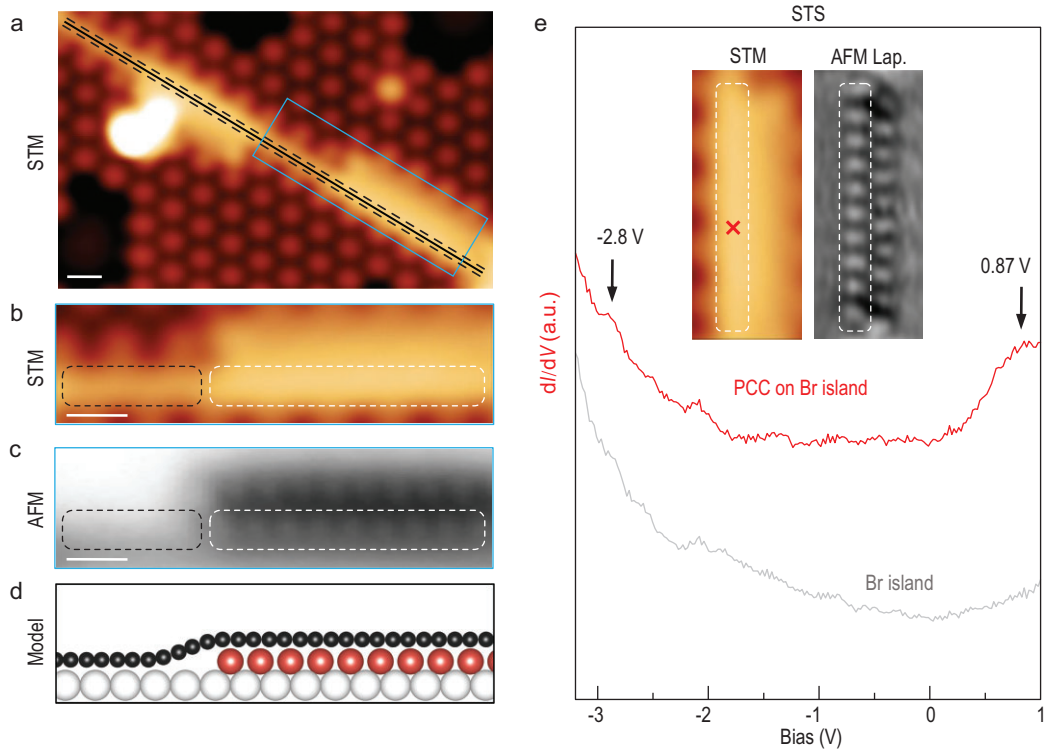

Figure 4. Characterization of the electronic properties of partially decoupled polyynic carbon chains. (a) An STM image of a PCC which is partially decoupled by Br atoms. A chemical structure is overlaid as a guide. (b–d) The STM image (b), AFM image (c), and schematic model (d) of partially decoupled PCC outlined by a blue contour in (a). The PCC segments on Br island and on Au(111) are indicated by white and black contours, respectively, in (b, c). Black, red, and white balls represent C, Br, and Au atoms, respectively. (e) The d*I*/d*V* spectrum of the PCC segment on Br island acquired at the position indicated by the red cross in the inserted STM image (red curve) and the reference spectrum taken on the Br island (grey curve). The spectra are vertically shifted for clarity. All the STM images are taken at $V = 0.40$ V, $I_t = 100$ pA. The AFM image (c) is recorded with a Br-functionalized tip at tip offset $\Delta z = -160$ pm with respect to an STM set point ($V = 0.40$ V, $I_t = 100$ pA). Scale bars: 0.5 nm.

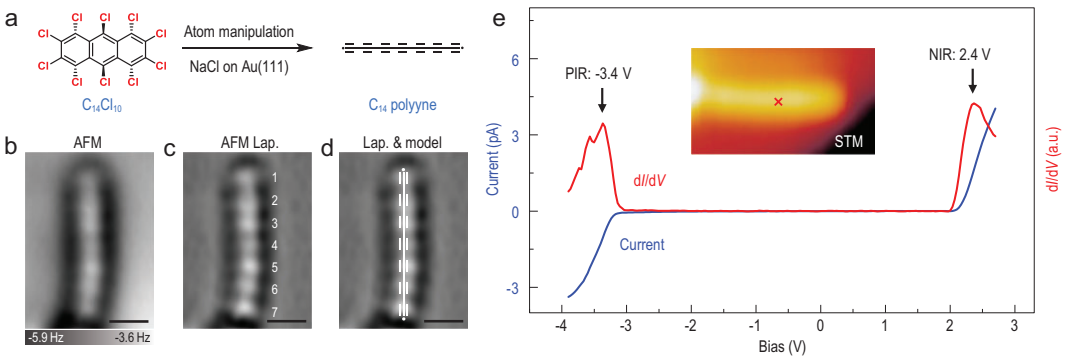

Figure 5. On-surface synthesis and characterization of a C_{14} polyyne via tip-induced dehalogenation and ring-opening of $C_{14}Cl_{10}$ on NaCl/Au(111). (a) Scheme of the formation of C_{14} polyyne. (b–d) AFM image (b) and Laplace-filtered AFM images (c, d) of a polyyne with 7 alkyne units. The chemical structure is overlaid in (d) as a guide. (e) The d*I*/d*V* spectrum of C_{14} polyyne (red curve) on NaCl/Au(111) acquired at the position indicated by the red cross in the inserted STM image along with the corresponding constant-height current spectrum (blue curve). AFM images were recorded with a CO-terminated tip at tip offset $\Delta z = -50$ pm with respect to the STM set point ($I = 1$ pA, $V = 0.3$ V) above the NaCl surface. Scale bars: 0.5 nm.

(6.86 eV) compared to the uncapped C_{14} polyyne with one radical at each end (5.48 eV) (Fig. S10). This finding also serves as evidence that the on-surface synthesized C_{14} polyyne was a pure carbon chain.

CONCLUSION

In summary, we have synthesized a polyynic carbon chain consisting of ∼60 contiguous alkyne units by debrominative coupling of C_4Br_6 molecules and subsequent demetallization on the Au(111) surface. The polyynic structure of PCCs was well-revealed by bond-resolved AFM. Moreover, a specific C_{14} polyyne was also successfully synthesized via atomic manipulation on a NaCl/Au(111) surface at 4.7 K, and a band gap of 5.8 eV was measured by STS. Our results provide bond-resolved experimental insights into the structure of the polyynic carbon chains and open an avenue for the synthesis and characterization of long polyynes without endgroups.

METHODS

STM and AFM measurements

The experiments were carried out in a low-temperature STM/nc-AFM (CreaTec) under ultra-high vacuum conditions (base pressure below 1×10^{-10} mbar). Au(111) single crystals purchased from MaTeck were used as substrates for the growth of PCCs. Preparation of clean Au(111) surfaces was achieved by cycles of Ar^+ ion sputtering and annealing at 850 K. The C_4Br_6 precursors were deposited (evaporator temperature 300 K) onto the clean Au(111) surface held at room temperature. After deposition, the sample was post-annealed to 380 K for 120 min to complete the reactions. $C_{14}Cl_{10}$ precursors were deposited (evaporator temperature 380 K) on cold NaCl/Au(111) surface held at 6 K. NaCl films were grown on Au(111) held at room temperature, resulting in islands of two and three monolayer thickness.

STM images were acquired in the constant-current mode at sample temperatures of 4.8 K. Non-contact AFM measurements were performed with a Pt/Ir tip attached to a tuning fork sensor. The tip was functionalized by controlled picking up of a CO molecule [24] (Fig. 5) or a Br atom [29] (other figures) at the tip apex from Au(111). CO molecules for tip modification were dosed onto the cold sample via a leak valve. We used a qPlus sensor [30] with a resonance frequency $f_0 = 29.49$ kHz, quality factor $Q \approx 45\,000$ and a spring constant $k \approx 1800$ N/m operated in frequency-modulation mode [31]. AFM images were acquired in constant-height mode at $V = 0$ V and an oscillation amplitude of $A = 1$ Å. The tip-height offsets Δz for constant-height AFM images are defined as the offset in tip-sample distance relative to the STM set point at the Au(111) surface. The positive (negative) values of Δz correspond to the tip-sample distance as increased (decreased) with respect to the STM set point.

The differential conductance (dI/dV) measurements were performed in the low-temperature STM/AFM at 4.8 K via the lock-in technique with a peak-to-peak bias-voltage modulation of 20 mV at a frequency of 768 Hz. The tips for dI/dV measurements are the same CO/Br-functionalized tips used for high-resolution AFM imaging. All the dI/dV maps were acquired in constant-height mode.

Theoretical calculations

The structural optimizations of PCCs and organometallic polyynes on Au(111) were performed in the framework of DFT by using the Vienna *ab initio* simulation package (VASP) [32,33]. The projector-augmented wave method [34,35] was used to describe the interaction between ions and electrons, and the Perdew-Burke-Ernzerhof generalized gradient approximation (GGA) exchange-correlation functional was employed [36]. The dispersion-corrected DFT-D3 method [37] was used to consider the van der Waals interactions. The Tersoff-Hamann method [38] was used to obtain the simulated STM images. ωB97XD exchange-correlation functional [39] in conjunction with def2-TZVP [40] basis sets was used for the electronic HOMO–LUMO gaps of the C_{14} polyyne using the Gaussian 16 program package [41] combined with Multiwfn 3.8 code and Visual Molecular Dynamics (VMD 1.9) [42].

Synthesis of precursors

1,1,2,3,4,4-Hexabromobutadiene (C_4Br_6) precursor was prepared using published procedures, as summarized in the Supplementary information; the characterization data match those previously reported [43,44]. Decachloroanthracene ($C_{14}Cl_{10}$) precursor was synthesized using procedures in ref. [45].

CODE AVAILABILITY

The Multiwfn software package is available at http://sobereva.com/multiwfn/.

SUPPLEMENTARY DATA

Supplementary data are available at *NSR* online.

FUNDING

This work was supported by the National Natural Science Foundation of China (22125203 and 21790351).

AUTHOR CONTRIBUTIONS

W.X. conceived and supervised the experiments; W.G., F.K. and L.S. performed the SPM experiments; W.Z. synthesized the precursor monomers; W.G. carried out the DFT calculations; all authors contributed to writing the manuscript.

***Conflict of interest statement*:** None declared.

REFERENCES

1. Kroto HW, Heath JR, O'Brien SC *et al.* C60: buckminsterfullerene. *Nature* 1985; **318**: 162–3.
2. Iijima S. Helical microtubules of graphitic carbon. *Nature* 1991; **354**: 56–8.
3. Iijima S and Ichihashi T. Single-shell carbon nanotubes of 1-nm diameter. *Nature* 1993; **363**: 603–5.
4. Novoselov KS, Geim AK, Morozov SV *et al.* Electric field effect in atomically thin carbon films. *Science* 2004; **306**: 666–9.
5. Hirsch A. The era of carbon allotropes. *Nat Mater* 2010; **9**: 868–71.
6. Hou L, Cui X, Guan B *et al.* Synthesis of a monolayer fullerene network. *Nature* 2022; **606**: 507–10.
7. Meirzadeh E, Evans AM, Rezaee M *et al.* A few-layer covalent network of fullerenes. *Nature* 2023; **613**: 71–6.
8. Goresy AE and Donnay G. A new allotropic form of carbon from the ries crater. *Science* 1968; **161**: 363–4.
9. Whittaker AG and Kintner PL. Carbon: observations on the new allotropic form. *Science* 1969; **165**: 589–91.
10. Liu M, Artyukhov VI, Lee H *et al.* Carbyne from first principles: chain of C atoms, a nanorod or a nanorope. *ACS Nano* 2013; **7**: 10075–82.
11. Karpfen A. *Ab initio* studies on polymers. I. The linear infinite polyyne. *J Phys C: Solid State Phys* 1979; **12**: 3227–37.
12. Gao Y and Tykwinski RR. Advances in polyynes to model carbyne. *Acc Chem Res* 2022; **55**: 3616–30.
13. Gibtner T, Hampel F, Gisselbrecht JP *et al.* End-cap stabilized oligoynes: model compounds for the linear sp carbon allotrope carbyne. *Chemistry* 2002; **8**: 408–32.
14. Zheng Q, Bohling JC, Peters TB *et al.* A synthetic breakthrough into an unanticipated stability regime: a series of isolable complexes in which C_6, C_8, C_{10}, C_{12}, C_{16}, C_{20}, C_{24}, and C_{28} polyynediyl chains span two platinum atoms. *Chem Eur J* 2006; **12**: 6486–505.
15. Chalifoux WA and Tykwinski RR. Synthesis of extended polyynes: toward carbyne. *C R Chim* 2009; **12**: 341–58.
16. Chalifoux WA and Tykwinski RR. Synthesis of polyynes to model the *sp*-carbon allotrope carbyne. *Nat Chem* 2010; **2**: 967–71.
17. Gao Y, Hou Y, Gordillo Gámez F *et al.* The loss of endgroup effects in long pyridyl-endcapped oligoynes on the way to carbyne. *Nat Chem* 2020; **12**: 1143–9.
18. Shi L, Rohringer P, Suenaga K *et al.* Confined linear carbon chains as a route to bulk carbyne. *Nat Mater* 2016; **15**: 634–9.
19. Sun Q, Cai L, Wang S *et al.* Bottom-up synthesis of metalated carbyne. *J Am Chem Soc* 2016; **138**: 1106–9.
20. Yu X, Li X, Lin H *et al.* Bond-scission-induced structural transformation from cumulene to diyne moiety and formation of semiconducting organometallic polyyne. *J Am Chem Soc* 2020; **142**: 8085–9.
21. Yu X, Sun Q, Liu M *et al.* Lattice-directed selective synthesis of acetylenic and diacetylenic organometallic polyynes. *Chem Mater* 2022; **34**: 1770–7.
22. Gao W, Kang F, Qiu X *et al.* On-surface debromination of C_6Br_6: C_6 ring versus C_6 chain. *ACS Nano* 2022; **16**: 6578–84.
23. Grill L, Dyer M, Lafferentz L *et al.* Nano-architectures by covalent assembly of molecular building blocks. *Nat Nanotechnol* 2007; **2**: 687–91.
24. Gross L, Mohn F, Moll N *et al.* Chemical structure of a molecule resolved by atomic force microscopy. *Science* 2009; **325**: 1110–4.
25. de Oteyza DG, Gorman P, Chen YC *et al.* Direct imaging of covalent bond structure in single-molecule chemical reactions. *Science* 2013; **340**: 1434–7.
26. Pavliček N, Gawel P, Kohn DR *et al.* Polyyne formation via skeletal rearrangement induced by atomic manipulation. *Nat Chem* 2018; **10**: 853–8.
27. Sun Q, Cai L, Ma H *et al.* Dehalogenative homocoupling of terminal alkynyl bromides on Au(111): incorporation of acetylenic scaffolding into surface nanostructures. *ACS Nano* 2016; **10**: 7023–30.
28. Dou W, Wu M, Song B *et al.* High-yield production of quantum corrals in a surface reconstruction pattern. *Nano Lett* 2023; **23**: 148–54.
29. Mohn F, Schuler B, Gross L *et al.* Different tips for high-resolution atomic force microscopy and scanning tunneling microscopy of single molecules. *Appl Phys Lett* 2013; **102**: 073109.
30. Giessibl FJ. High-speed force sensor for force microscopy and profilometry utilizing a quartz tuning fork. *Appl Phys Lett* 1998; **73**: 3956–8.
31. Albrecht TR, Grütter P, Horne D *et al.* Frequency modulation detection using high-Q cantilevers for enhanced force microscope sensitivity. *J Appl Phys* 1991; **69**: 668–73.
32. Kresse G and Hafner J. *Ab initio* molecular dynamics for open-shell transition metals. *Phys Rev B* 1993; **48**: 13115–8.
33. Kresse G and Furthmuller J. Efficient iterative schemes for *ab initio* total-energy calculations using a plane-wave basis set. *Phys Rev B* 1996; **54**: 11169–86.
34. Blöchl PE. Projector augmented-wave method. *Phys Rev B* 1994; **50**: 17953–79.
35. Kresse G and Joubert D. From ultrasoft pseudopotentials to the projector augmented-wave method. *Phys Rev B* 1999; **59**: 1758–75.
36. Perdew JP, Burke K, Ernzerhof M. Generalized gradient approximation made simple. *Phys Rev Lett* 1996; **77**: 3865–8.

37. Grimme S, Antony J, Ehrlich S *et al.* A consistent and accurate *ab initio* parametrization of density functional dispersion correction (DFT-D) for the 94 elements H-Pu. *J Chem Phys* 2010; **132**: 154104.
38. Tersoff J and Hamann D. Theory of the scanning tunneling microscope. *Phys Rev B* 1985; **31**: 805–13.
39. Chai J and Head-Gordon M. Long-range corrected hybrid density functionals with damped atom–atom dispersion corrections. *Phys Chem Chem Phys* 2008; **10**: 6615.
40. Weigend F and Ahlrichs R. Balanced basis sets of split valence, triple zeta valence and quadruple zeta valence quality for H to Rn: design and assessment of accuracy. *Phys Chem Chem Phys* 2005; **7**: 3297.
41. Frisch MJ, Trucks GW, Schlegel HB *et al. Gaussian 16 Rev. C.01*. Gaussian, Inc.: Wallingford, CT 2016.
42. Humphrey W, Dalke A, Schulten K. VMD: visual molecular dynamics. *J Mol Graphics* 1996; **14**: 33–8.
43. Liu P, Li L, Webb JA *et al.* Tetrabromobutatriene: completing the perhalocumulene series. *Org Lett* 2004; **6**: 2081–3.
44. Straus F, Kollek L, Hauptmann H. Über Dihalogen-diacetylene (zugleich II. Mitteilung über den Ersatz positiven Wasserstoffs durch Halogen). *Ber Dtsch Chem Ges B* 1930; **63**: 1886–99.
45. Dobrowolski MA, Cyrański MK, Wróbel Z. Cyclic π-electron delocalization in non-planar linear acenes. *Phys Chem Chem Phys* 2016; **18**: 11813–20.